Magneto–Optical Properties of Tb^{3+} Ions in Crystals of Aluminum Borate

A.A. Prokhorov[a,*], R. Minikayev[b], T. Zajarniuk[b], A. Szewczyk[b], J. Lančok[a] and A.D. Prokhorov[c]

[a] *Institute of Physics AS CR, Na Slovance 2, 18221 Prague, Czech Republic*
[b] *Institute of Physics PAS, al. Lotnikow 32/46, PL 02668, Warsaw, Poland*
[c] *A.A. Galkin Donetsk Physico-Technical Institute, R. Luxembourg 72, 83114 Donetsk*

Received: 10.01.2022 & Accepted: 22.02.2022

Doi: 10.12693/APhysPolA.141.523 *e-mail: prokhorov@fzu.cz

New data on the state of Tb^{3+} doping ions in the $EuAl_3(BO_3)_4$ single crystals have been obtained by studying the electron paramagnetic resonance spectra within the X band and optical absorption spectra at 4 K in the visible range. Additionally, the specific heat of these crystals was measured and analyzed. It has been shown that the Tb^{3+} ions substitute the trivalent europium ones and lower crystal symmetry. In the crystal field, the ground multiplet of Tb^{3+} splits in such a way that two singlets located in close proximity are the lowest energy levels. It has been shown that the temperature dependence of the linewidth can be described by the exponential function, which is characteristic of the Aminov–Orbach processes.

topics: EPR spectra, rare-earth, aluminum borates, spin Hamiltonian parameters

1. Introduction

Borates of the formula $REM_3(BO_3)_4$, where RE is a rare-earth ion or yttrium, and M can be Al, Fe, Ga, or Cr, display a set of features, e.g., significant luminescent and non-linear optical properties, that make them attractive from the viewpoint of basic research and application. A high concentration of doping ions is not accompanied by concentration quenching in aluminum borates. The physical and chemical properties of these crystals make them promising media for solid-state lasers. Single crystal aluminum borates provide effective transformation of the frequencies of laser radiation with an efficiency that exceeds the analogous parameters of the other known media. Crystals of borates doped by ytterbium were employed to obtain the laser pulses of femtosecond duration. Laser radiation of the wavelength of 1.5 μm, generated by the erbium-doped crystals of this family, shows small propagation losses in the atmosphere and found application in medicine [1–6].

Interaction between the iron ions in quasi-one-dimensional chains of $REFe_3(BO_3)_4$ (where RE means rare-earth elements) results in an antiferromagnetic ordering in the 30–37 K range [7]. Weak spin-spin interaction between the Tb^{3+} ions forms a magnetic ordering in $TbAl_3(BO_3)_4$ at the temperature of 0.68 K [8]. Moreover, the magnetoelectric effect with a very large electric polarization, larger than in other multiferroics, found in some crystals of borates is a very important property of these materials [9–11]. A series of works is devoted to the study of EPR spectra in aluminum borates [12–36]. Much less attention was paid to the crystals with M = Ga ($REGa_3(BO_3)_4$), which may also demonstrate interesting properties [37–41]. Both the $REGa_3(BO_3)_4$ crystals and the thoroughly studied aluminum borates crystalize in the same structure described by the space group $R32$. It is important that the terbium ions in borates have an energy spectrum that allows using these materials as a basis for solid-state lasers and scintillators. The luminescence spectra of the Tb^{3+} in the visible band can be applied in luminophores.

The present paper reports the results of studies of the ground state of a trivalent terbium ion incorporated into the lattice of $EuAl_3(BO_3)_4$ by electron paramagnetic resonance.

2. Crystal growth and structural analysis

$EuAl_3(BO_3)_4$:0.2%Tb^{3+} doped crystal was grown by the spontaneous solution-melt crystallization method (for more details, see [12]). The structural analysis of the sample was done by the X-ray powder diffraction method. The XRD measurements were carried out using the X'Pert Pro Alpha1 MPD (Panalytical) laboratory diffractometer. The diffraction pattern contained two groups of peaks, which proved that the investigated sample consisted of two phases, i.e., the main phase being

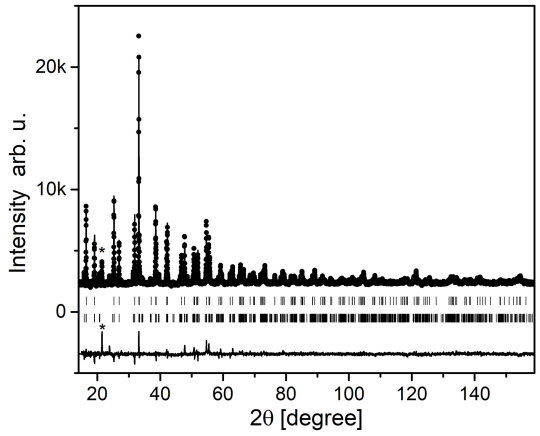

Fig. 1. Rietveld refinement result for Tb^{3+} doped $EuAl_3(BO_3)_4$. Reflection positions are indicated by bars below the diffraction curve. The lower set of bars presents the reflections for the minor monoclinic phase.

TABLE I

The atomic positions in the two structures of $EuAl_3(BO_3)_4$:0.2%Tb^{3+} doped.

Name	Atomic positions		
	x	y	z
Eu	0	0	0
Al/Tb	0.5551±0.0007	0	0
B(1)	0	0	0.5
B(2)	0.446±0.0002	0	0.5
O(1)	0.8644±0.0006	0	0.5
O(2)	0.579±0.001	0	0.5
O(3)	0.4456±0.0006	0.1364±0.0006	0.5224±0.0008

in the huntite structure (space group $R32$) [42] and the minor phase in the $NdAl_3(BO_3)_4$ structure (space group $C12/c1$) [43]. The crystallographic structures of these phases were refined by the Rietveld method with the help of the Fullprof.2k program [44].

The graphical results of the Rietveld refinement are presented in Fig. 1, and the refined atomic positions for the main phase (huntite structure) are given in Table I. The obtained unit-cell parameters of the huntite phase are 9.3089 ± 0.0001 Å and 7.2686 ± 0.0001 Å for the a and c axes, respectively. These values are very close to the data for the $EuAl_3(BO_3)_4$ undoped material, reported earlier in [45]. The content of the second (minor) phase is about 12 at.%. For that phase, described by the space group $C12/c1$, the lattice parameters are equal to a=7.2254±0.0004 Å, b=9.3304±0.0005 Å, and c=11.0857±0.0006 Å and β=103.202±0.004°. The minor phase availability on diffraction pattern was caused by the inability to select the $R32$ type crystals only from the crystal mixture, which was powdered for XRD measurements. But for EPR and optical measurements, the $R32$ type crystals were selected by checking the purity of EPR spectra.

3. EPR measurements

The EPR spectrum of terbium ions was measured at low temperatures within the Q and X bands. The spectrum is composed of four lines of superfine structure, as presented in Fig. 2 ($EuAl_3(BO_3)_4$). The angular dependence of the spectra demonstrated that the same spectrum is registered at any angle, as in the case of other rare-earth ions incorporated by the tested crystals [22, 30–34]. Ions of Tb^{3+} substitute for Eu^{3+} at a ratio of 1:500 in the matrix. The ions of Tb^{3+} are found in the nodes of D_3 symmetry. The electron configuration of trivalent terbium is $4f^8$. In the trigonal field, the ground multiplet $^7F_6$ is split into 6 singlets and 4 doublets.

In the energy spectrum of Tb^{3+} in the crystal field of the borates, two singlets of the lowest energy are slightly split, and the transitions between them are allowed. To describe the EPR spectra theoretically, the spin Hamiltonian was written in the form [46, 47]

$$H = g\beta H_z S_z + A\, S_z I_z + \Delta\, S_x, \qquad (1)$$

where the electron spin is $S = 1/2$, nuclear spin is $I = 3/2$, g is the effective g-factor, β is the Bohr magneton, A is the constant of hyperfine interaction, and Δ is the parameter that characterizes splitting of the singlets in zero magnetic field.

The eigenvalues of the spin Hamiltonian (1) for arbitrary orientation of the magnetic field are

$$E = \pm\frac{1}{2}\sqrt{\left(g\beta H\, \cos\left(\Theta + A\, m\right)\right)^2 + \Delta^2}, \qquad (2)$$

where Θ is an angle between C3 axis and magnetic field direction, and m takes half-integer values from the range from $+3/2$ to $-3/2$. When the magnetic field is aligned with Z-axis (C_3), the transitions take place if

$$h\nu = \sqrt{\left(g\beta\, H_z + A\, m\right)^2 + \Delta^2}, \qquad (3)$$

where ν is the frequency of the applied microwave field.

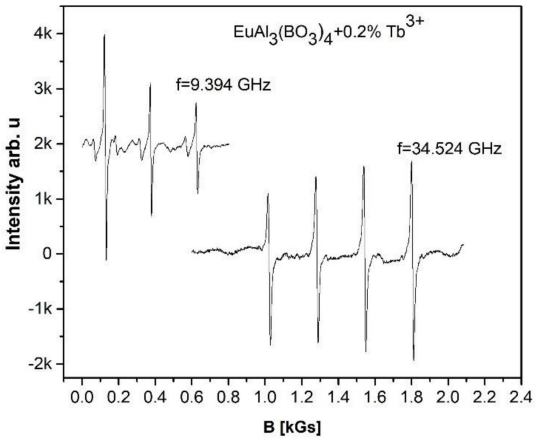

Fig. 2. EPR spectrum of the Tb^{3+} ion in the $EuAl_3(BO_3)_4$ crystal at two frequencies f=9.394 GHz and f=34.524 GHz.

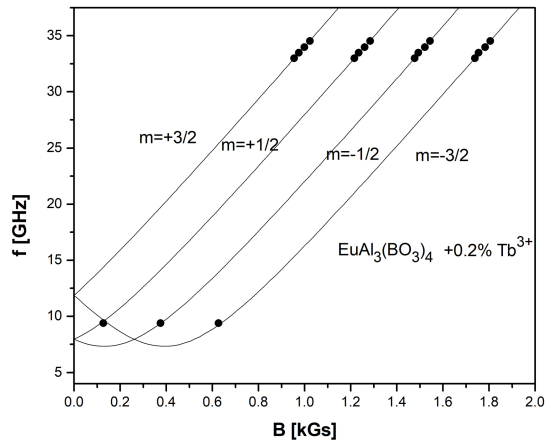

Fig. 3. Dependence of the resonant frequency f of the transitions between the hyperfine structure levels of the Tb^{3+} ion in $EuAl_3(BO_3)_4$ crystal on the magnetic field.

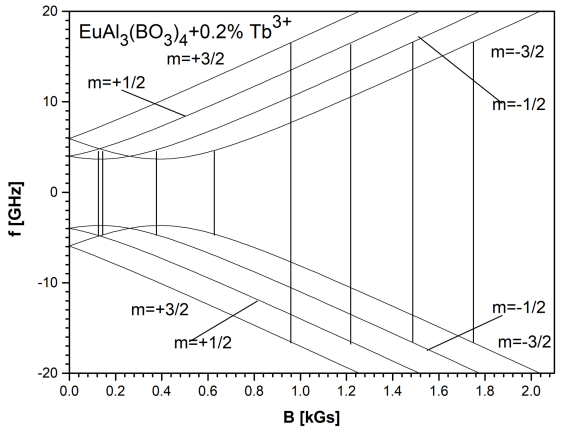

Fig. 4. Two lowest energy levels of the Tb^{3+} ion in the $EuAl_3(BO_3)_4$ crystal as a function of the magnetic field. Transitions between the levels of the hyperfine structure in the Q and X bands are shown.

The measurements have been performed for a set of frequencies. Specific features of the used spectrometer did not allow for varying the frequency in a wide range. We used one frequency from the X band. A possibility was found to vary the frequency within the Q band to some extent and to perform the measurements at four frequencies. To evaluate the parameters, the registered frequency and the magnetic field were substituted into (3), and the fitting procedure was carried out.

In Fig. 3, the dependence of the resonance frequencies of the transitions between the levels of the hyperfine structure of Tb^{3+} in $EuAl_3(BO_3)_4$ is presented as a function of the magnetic field parallel to the C_3 axis.

The spin Hamiltonian parameters and the frequencies of the transitions corresponding to the zero field are listed in Table II.

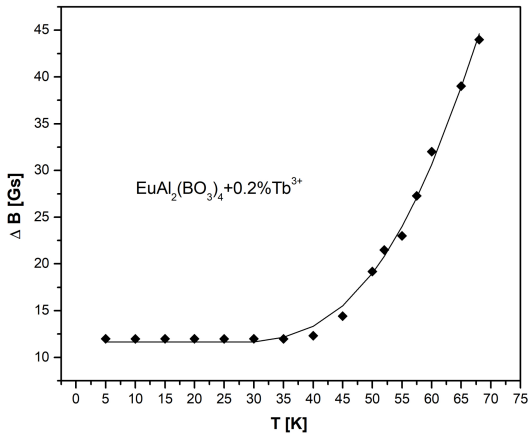

Fig. 5. Dependence of Tb^{3+} ion line width on temperature in the $EuAl_3(BO_3)_4$ crystals.

TABLE II

The values of parameters g, Δ, A, ν_1 and ν_2 for $EuAl_3(BO_3)_4$:0.2%Tb^{3+}.

Parameter	Value
g	17.064 ± 0.019
Δ [GHz]	7.333 ± 0.016
A [GHz]	6.231 ± 0.012
ν_1 [GHz]	7.967
ν_2 [GHz]	11.879

When analyzing the spectrum of Tb^{3+} in $EuAl_3(BO_3)_4$, it can be noted that only three of four absorption lines were registered in the low-frequency part of the spectrum. This fact is attributed to the casual coincidence of two transitions that are presented in Fig. 4, namely, for $m = -3/2$ and $m = +1/2$. In such case, (3) can be approximated as $h\nu = \sqrt{A^2 + \Delta^2}$.

Rare-earth ions that are characterized by a $4f$ valent shell are strongly coupled to lattice oscillations [48]. As a result, the time of spin-lattice relaxation is short, and EPR spectra can be registered at low temperatures only. The temperature dependence of the linewidth to evaluate the spin-lattice relaxation time and to determine the relaxation mechanisms. The temperature dependence of the linewidth was measured for the external magnetic field parallel to the C_3 axis. The linewidth was determined as the distance between the extreme derivatives of the absorption line. Spin-phonon contribution to the linewidth was calculated by subtraction of the temperature-independent component, i.e., of the linewidth at helium temperature, from the total linewidth determined.

The temperature dependence of the linewidth for the crystal is presented in Fig. 5. This dependence is well described by the exponential function

$$\Delta H_{pp}(T) = 12 + 1.4 \times 10^3 \exp\left(-\frac{262}{T}\right). \qquad (4)$$

Usually, Δ is indicative of the energy level participating in Aminov–Orbach relaxation in the ion energy spectrum. We suppose that the value of Δ obtained by fitting the theoretical function to the experimental data is an average, effective value because other energy levels of the multiplet can also participate in relaxation at temperatures below 65 K.

The experimentally found energy levels are measured in cm^{-1}. As the performed specific heat studies showed, the Debye temperature of the studied crystals is of the order of $\theta_\mathrm{D} \approx 378$ K. Thus, the majority of energy levels of the ground multiplet can contribute to the spin-lattice relaxation that determines the temperature dependence of the linewidth.

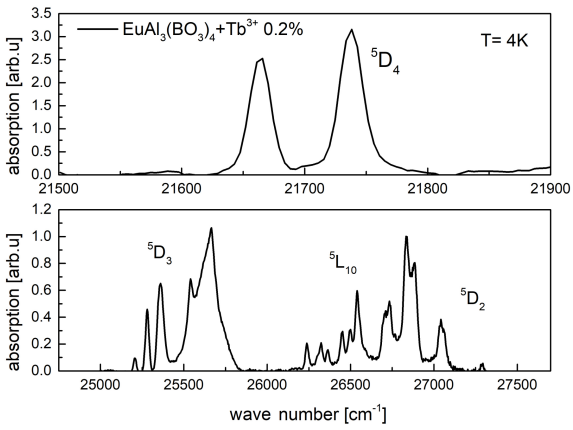

Fig. 6. Optical absorption spectra of the Tb^{3+}:$EuAl_3(BO_3)_4$ crystal at low temperature.

4. Optical absorption and specific heat

Optical absorption measurements were performed in a temperature range from 3.5 to 300 K using the cryostat with the ITC4 programmed temperature controller (Au/Fe-chromel thermocouple). The spectra were analyzed with a Zeiss model SPM2 grating monochromator (setting to a spectral bandwidth of 2 cm^{-1}), in which a cooled photomultiplier is used as the detector. The SRS 250 boxcar integrator has averaged the resulting signal. A continuous flow helium cryostat (Oxford, model CF 1104) was used for low-temperature measurements.

The results of the optical absorption measurements of the $EuAl_3(BO_4)_3$ single crystal doped with 0.2% mole Tb^{3+} at low temperature are shown in Fig. 6. Four main groups of absorption peaks, i.e., ${}^5D_4$, ${}^5D_3$, ${}^5L_{10}$, and ${}^5D_2$, were found in the range of wavelengths studied. These groups are centered at about 21700, 25500, 26300, and 26800 cm^{-1}, respectively. They correspond to the transitions between the energy levels of Tb^{3+} ions in the crystal. The positions of the multiples for optical spectra in $EuAl_3(BO_3)_4$:Tb^{3+} are very similar to the positions of the multiplets in the crystal $TbAl_3(BO_3)_4$ [49]. The consistency of the positions of the multiplets can be explained by the different surroundings of the Tb^{3+} ions. Terbium ions in the studied material occur as an impurity and do not occupy all positions of the rare-earth in this material. Therefore, the values of the parameters of the crystal field are also different, which results in different splitting of energy levels. The complete splitting of the multiplets into individual levels was not achieved due to the small size of the studied samples.

The specific heat measurements have been carried out using the heat capacity option of the physical property measurement system (PPMS) made by Quantum Design, in which the relaxation method of specific heat measurement is used. The sample was mounted on a sapphire plate using a possibly small amount of the vacuum grease "Apiezon N" necessary to assure good thermal contact between the sample and the calorimetric sapphire plate. The grease contribution to the measured specific heat was estimated and subtracted. The estimated uncertainty of the determined specific heat values was $\sim 2\%$. The specific heat was measured every 0.5 K in the low-temperature range, i.e., below 20 K, approximately every 1 K in the range from 20 to 100 K, every 2 K for temperatures from 100 to 200 K, and each 5 K for the range from 200 to 300 K. The studies were done from 2 to 300 K for both crystals in zero magnetic field B.

The measured temperature dependence of the specific heat of Tb^{3+}:$EuAl_3(BO_3)_4$ is presented in Fig.7. In order to analyze the experimental dependence theoretically, we assumed that the phonon specific heat, which is the main contribution to the specific heat of the compounds studied, is given by

$$C_{ph}(T) = \frac{k_\mathrm{B} N_\mathrm{A}}{2} \frac{3n_\mathrm{D}}{1-\alpha T} \left(\frac{T}{\theta_\mathrm{D}}\right)^3 \int_0^{\theta_\mathrm{D}/T} \mathrm{d}x \, \frac{x^4 \, \mathrm{e}^x}{(\mathrm{e}^x - 1)^2} + \sum_{i=1}^{n_\mathrm{o}} n_i \left(\frac{\theta_i}{T}\right)^2 \frac{\exp\left(\frac{\theta_i}{T}\right)}{\left(\exp\left(\frac{\theta_i}{T}\right) - 1\right)^2}, \tag{5}$$

where k_B is the Boltzmann's constant, θ_D is the Debye temperature, n_D denotes the number of the phonon modes that can be considered within the Debye model, n_o is the number of nondispersive optical branches that can be treated within the Einstein model, θ_i is the energies of particular Einstein branches (expressed in temperature units), and n_i denotes the number of optical modes assigned to

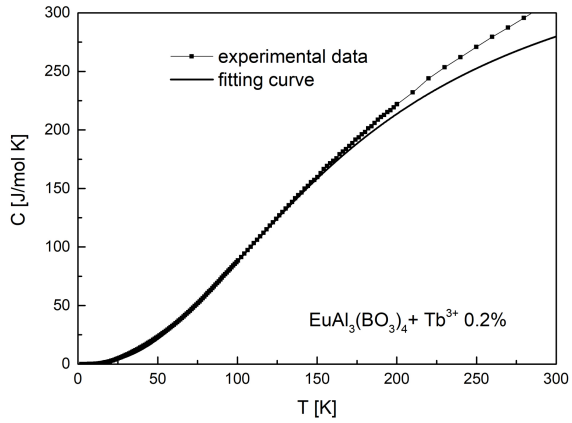

Fig. 7. Specific heat of the Tb^{3+}:$EuAl_3(BO_3)_4$ single crystal. The black line presents the total specific heat (experimental data), measured in $B = 0$ with standard calorimeter, and the line presents the estimated C_{ph} contribution.

the i-th branch. In the procedure of fitting (5) to the experimental data, the energies of optical phonons were determined. The best fit was achieved for Einstein branches of optical phonons of the fitted energies 105, 212, 277, 354, 437, 498, 592, 666, and 700 K. As the result of fitting, the following parameter values were obtained: $\alpha = 0.000034$, $\theta_D \approx 378$ K, $\theta_D \approx (385 \pm 10)$ K, and $n_D = 8$. The theoretical dependence $C_{ph}(T)$ determined this way is plotted in Fig. 7 with the solid line.

In the result of fitting (4) to the low-temperature part of the experimental data only, the Debye temperatures $\theta_D \approx 378$ K was determined. Estimation of the Debye temperature is a valuable result because the Debye temperature is the important parameter, entering expressions describing various physical properties, e.g., the expression describing temperature-dependent line broadening for radiative transitions, related to the electron-phonon coupling.

5. Conclusion

The structural analysis of the $EuAl_3(BO_3)_4$ sample doped by 0.2% of Tb^{3+} ions has been performed using the XRD technique, which showed that the huntite type structure is the main crystallographic phase of the studied crystal. As follows from the angular dependences of the EPR spectrum measured, the doping trivalent terbium ions substitute the trivalent europium ions in the lattice. The measurements performed at different frequencies allowed us to evaluate the energy distance between the two singlets of the ground state of Tb^{3+}, the g-factors, and the parameters of hyperfine splitting, as well as to calculate the magnetic field dependence of the energy levels. It has been demonstrated that the temperature dependence of the linewidth can be described by the exponential function, which is characteristic of the Aminov–Orbach processes. Moreover, the optical absorption and the Debye temperature of the Tb:$EuAl_3(BO_3)_4$ crystal were studied.

Acknowledgments

The EPR measurements were carried out within the SAFMAT infrastructure at FZU CAS. This research was supported partially by the Czech Science Foundation (GACR), Project No. 20-21069S, and by the National Science Centre, Poland, under project No. 2018/31/B/ST3/03289. We acknowledge the Operational Program Research, Development and Education financed by European Structural and Investment Funds and the Czech Ministry of Education, Youth and Sports Project SOLID21 CZ.02.1.01/0.0/0.0/16_019/0000760.

References

[1] Junhai Liu, Yong Wan, Xueping Tian, Zhichao Zhou, Wenjuan Han, Jing Li, Huaijin Zhang, Jiyang Wang, *Appl. Phys. B* **111**, 233 (2013).

[2] D. Jaque, J. Capmany, J. Garcıia Solé, *Appl. Phys. Lett.* **75**, 325 (1999).

[3] W. Liang, X.H. Zhang, J. Xia, G.Y. Jin, L.J. Xu, G.C. Sun, Z.M. Zhao, *Laser Phys.* **21**, 861 (2011).

[4] P. Wang, J.M. Dawes, P. Dekker, J.A. Piper, *Opt. Commun.* **174**, 467 (2000).

[5] P.A. Burns, J.M. Dawes, P. Dekker, J.A. Piper J. Li, J. Wang, *Opt. Commun.* **207**, 315 (2002).

[6] N.I. Leonyuk, V.V. Maltsev, E.A. Volkova, O.V. Pilipenko, E.V. Koporulina, V.E. Kisel, N.A. Tolstik, S.V. Kurilchik, N.V. Kuleshov, *Opt. Mater.* **30**, 161 (2007).

[7] Y. Hinatsu, Y. Doi, K. Ito, M. Wakeshima, A. Alemi, *J. Solid State Chem.* **172**, 438 (2003).

[8] V.V. Bedarev, M.I. Paschenko, M.I. Kobets et al., *Low Temp. Phys.* **41**, 534 (2015).

[9] A.I. Begunov, A.A. Demidov, I.A. Gudim, E.V. Eremin, *JEPT Lett.* **97**, 528 (2013).

[10] R.P. Chaudhury, B. Lorenz, Y.Y. Sun, L.N. Bezmaternykh, V.L. Temerov, C.W. Chu, *Phys. Rev. B* **81**, 220402 (2010).

[11] A.M. Kadomtseva, Yu.F. Popov, G.P. Vorob'ev et al., *Phys. Rev. B* **89**, 014418 (2014).

[12] Xueyuan Chen, Zundu Luo, D. Jaque, J.J. Romero, J. Garcia Sole, Yidong Huang, Aidong Jiang, Chaoyang Tu, *J. Phys.: Condens. Matter* **13**, 1171 (2001).

[13] D. Jaque, O. Enguita, J.G. Sole, A.D. Jiang, Z.D. Luo, *Appl. Phys. Lett.* **76**, 2176 (2000).

[14] A. Brenier, Chaoyang Tu, Zhaojie Zhu, Jianfu Li, Yan Wang, Zhenyu You, BaiChang Wu, *Appl. Phys. Lett.* **84**, 16 (2004).

[15] A.D. Balaev, L.N. Bezmaternykh, I.A. Gudim, V.L. Temerov, S.G. Ovchinnikov, S.A. Kharlamova, *J. Magn. Magn. Mater.* **258**, 532 (2003).

[16] S.A. Kharlamova, S.G. Ovchinnikov, A.D. Balaev, M.F. Thomas, I.S. Lyubutin, A.G. Gavriliuk, *J. Exp. Theor. Phys.* **101**, 1098 (2005).

[17] A.A. Prokhorov, A.D. Prokhorov, L.F. Chernush, V.P. Dyakonov, H. Szymczak, A. Dejneka, *Phys. Scr.* **90**, 065804 (2015).

[18] A.M. Vorotynov, G.A. Petrakovskii, Ya.G. Shiyan, L.N. Bezmaternykh, V.E. Temerov, A.F. Bovina, P. Aleshkevych, *Phys. Solid State* **49**, 463 (2007).

[19] C. Rudowicz, P. Gnutek, M. Acikgoz, *Opt. Mater.* **46**, 254 (2015).

[20] M. Acikgoz, P. Gnutek, C. Rudowicz, *Opt. Mater.* **36**, 1342 (2014).

[21] A.A.Prokhorov, L.F. Chernush, V. Babin, M. Buryi, D. Savchenko, J. Lančok, M. Nikl, A.D.Prokhorov, *Opt. Mater.* **66**, 428 (2017).

[22] A.A. Prokhorov, L.F. Chernush, V.P. Dyakonov, H. Szymczak, A.D. Prokhorov, *J. Magn. Magn. Mater.* **420**, 285 (2016).

[23] J.P.R. Wells, M. Yamaga, T.P.J. Han, M. Honda, *J. Phys.: Condens. Mat.* **15**, 539 (2003).

[24] A.D. Prokhorov, E.E. Zubov, A.A. Prokhorov, L.F. Chernush, R. Minyakaev, V.P. Dyakonov, H. Szymczak, *Phys. Status Solidi B* **250**, 1331 (2013.

[25] A.A. Prokhorov, *J. Mater. Sci.* **51**, 4762 (2016).

[26] M. Acikgoz, C. Rudowicz, P. Gnutek, *Opt. Mater.* **73**, 124 (2017).

[27] V.A. Atsarkin, Vb. Kravchen, I.G. Matveeva, *Sov. Phys. Solid State* **9**, 2646 (1968).

[28] G. Wang, H.G. Gallagher, T.P.J. Han, B. Henderson, M. Yamaga, T. Yosida, *J. Phys.: Condens. Mat.* **9**, 1649 (1997).

[29] A. Watterich, P. Aleshkevych, M.T. Borowiec, T. Zayarnyuk, H. Szymczak, E. Beregi, L. Kovács, *J. Phys.: Condens. Mat.* **15**, 3323 (2003).

[30] A.D. Prokhorov, A.A. Prokhorov, L.F. Chernysh, P. Aleshkevich, V. Dyakonov, H. Szymczak, *J. Magn. Magn. Mater.* **326**, 162 (2013).

[31] A.D. Prokhorov, I.N. Krygin, A.A. Prokhorov, L.F. Chernush, P. Aleshkevich, V. Dyakonov, H. Szymczak, *Phys. Status Solidi A* **206**, 2617 (2009).

[32] A.D. Prokhorov, A.A. Prokhorov, L.F. Chernysh, V.P. Dyakonov, H. Szymczak, *J. Magn. Magn. Mater.* **323**, 1546 (2011).

[33] A.D. Prokhorov, A.A. Prokhorov, E.E. Zubov, L.F. Chernysh, *Low Temp. Phys.* **40**, 730 (2014).

[34] A.D. Prokhorov, A.A. Prokhorov, L.F. Chernush, R. Minyakaev, V.P. Dyakonov, H. Szymczak, *Phys. Status Solidi B* **251**, 201 (2014).

[35] A.A. Prokhorov, L.F. Chernush, R. Minyakaev, A. Mazur, T. Zajarniuk, A. Szewczyk, V. Dyakonov, J. Lančok, A.D. Prokhorov, *J. Alloy Compd.* **765**, 710 (2018).

[36] A.A. Prokhorov, L.F. Chernush, T.N. Melnik, R. Minikayev, A. Mazur, V. Babin, M. Nikl, J. Lančok, A.D. Prokhorov, *Sci. Rep.* **9**, 12787 (2019).

[37] A.A. Prokhorov, L.F. Chernush, R. Minikayev, J. Lancok, A.D. Prokhorov, *Acta Phys. Pol. A* **136**, 947 (2019).

[38] A.A. Prokhorov, E.E. Zubov, L.F. Chernush, R. Minikayev, V. Babin, M. Nikl, T. Zajarniuk, A. Szewczyk, D. Savchenko, J. Lančok, A.D. Prokhorov,, *Results Phys.* **19**, 103247 (2020).

[39] A.A. Prokhorov, R. Minikayev, D.V. Savchenko, J. Lancok, A.D. Prokhorov, *Mater. Chem. Phys.* **275**, 125251 (2022).

[40] S.N. Krylova, A.S. Aleksandrovsky, E.M. Roginskii, A.A. Krylov, I.A. Gudim, A.N. Vtyurin, *Ferroelectrics* **559**, 135 (2020).

[41] A.L. Freidman, A.A. Dubrovskii, V.L. Temerov, I.A. Gudim, *Phys. Solid State* **60**, 510 (2018).

[42] E.L. Belokoneva, A.V. Azizov, N.I. Leonyuk, M.A. Simonov, N.V. Belov, *J. Struct. Chem.* **22**, 476 (1981).

[43] E.L. Belokoneva, M.A. Simonov, A.V. Pashkova, T.I. Timchenko, N.V. Belov, *Dokl. Akad. Nauk SSSR* **255**, 854 (1980).

[44] J. Rodriguez-Carvajal, *Mater. Sci. Forum* **378**, 268 (2001).

[45] N.I. Leonyuk, L.I. Leonyuk, *Prog. Cryst. Growth Ch.* **31**, 179 (1995).

[46] J.S. Griffith, *Phys. Rev.* **132**, 316 (1963).

[47] P.A. Forrester, C.F. Hempstead, *Phys. Rev.* **126**, 923 (1962).

[48] S.A. Altshuler, B.M. Kozyrev, *Elektronny Paramagnitny Rezonans Soyedineniy Elementov Promezhutochnykh Grupp*, Nauka, Moskva, 1972.

[49] I. Couwenberg, K. Binnemans, H. De Leebeeck, C. Gorller-Walrand, J. Alloy Compd. **274**, 157 (1998).